Fuel 371 (2024) 131951

Contents lists available at ScienceDirect

Fuel

journal homepage: www.elsevier.com/locate/fuel

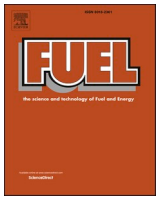

Full Length Article

Nitric oxide formation in flames of NH3/DME binary mixtures: Laser-induced fluorescence measurements and detailed kinetic analysis

Vladimir A. Alekseev, Christian Brackmann, Xin Liu, Elna J.K. Nilsson *

Division of Combustion Physics, Lund University, Box 118, 22100 Lund, Sweden

ARTICLE INFO

Keywords:
NH3
DME
NO formation
PLIF
Detailed chemistry
C-N interactions

ABSTRACT

Binary mixture of ammonia (NH_3) and dimethyl ether (DME) has been considered in literature as a potential fuel for practical use. Nitric oxide (NO) is a major product of combustion of NH_3-containing fuels, and its formation routes have to be comprehensively studied. In this work, concentration profiles of NO were experimentally measured in laminar axisymmetric flames using planar laser-induced fluorescence. The molar percentage of NH_3 in the NH_3/DME fuel mixture varied from 10% to 60%. Emission levels of NO have reached as much as around 1% for mixtures with around 50% NH_3. NO formation was analyzed with numerical simulations of 1D laminar flames and several detailed kinetic mechanisms. Modeling was performed in Chemkin with the steady-state burner-stabilized and free-propagating planar laminar flame reactor models. It was observed that the most recent versions of the contemporary NH_3/DME models are able to reproduce the experiments, and their predictions agree with each other due to similarities in the NH_3 submechanisms. Kinetic analysis has revealed some disagreement was observed in terms of how much direct chemical coupling between carbon- and nitrogen-containing species affects NO formation.

1. Introduction

In recent years, ammonia (NH3) has received substantial attention as a prospective fuel for internal combustion engines [1]. In most cases, the addition of a secondary hydrocarbon pilot fuel such as diesel [2,3], n-heptane [4] or dimethyl ether (DME) [5,6] is required due to the slow ignition of NH_3. Emissions in terms of nitric (NO, NO_2) and nitrous (N_2O) oxides are also commonly reported [2,4,7].

To separate the effects related to complex combustor geometries and turbulence from chemical kinetics, NO formation is studied in laminar flames, either by measuring emissions in the post-flame zone or by obtaining full NO profiles across the flame front.

Considering NO concentrations in products gases of laminar premixed flames, recent measurements are available for NH_3-H_2 [8,9], NH_3-CH_4 [8,10–12] and NH_3-DME [13] fuel mixtures. However, only Ramos et al. [10] implemented a flame geometry close to one-dimensional, which is desirable when NO formation is studied with detailed chemistry. Henshaw et al. [14] reported NO concentrations in flames stabilized on a heat flux burner, however, the maximal NH_3 fraction in the investigated NH_3-CH_4 mixtures was only 5 %.

Considering flame structure, the first studies of NH_3/H_2 [15] and NH_3/CH_4 [16] fuel mixtures were conducted at low pressures using probe sampling and mass spectrometry. The same technique was used to obtain profiles of major species, N_2O and NO in atmospheric-pressure NH_3/H_2/O_2/Ar flames [17] and later at pressures 4–6 atm [18]. The flame structure of NH_3-containing binary fuels has also been investigated with optical diagnostics. Yang et al. [19] implemented ultraviolet broadband absorption spectroscopy to measure NO, OH, NH and NH_3 in NH_3/CH_4 flames (10–50 % NH_3) stabilized on a McKenna burner at 1 atm. Rocha et al. [20] investigated NH_3/CH_4 fuel mixtures with 20–80 % of NH_3 and at various pressures, up to 3 atm. In order to resolve the reaction zone at high pressures, the flames were stabilized on a Bunsen-type burner, and 2D distributions of NH and NO were obtained with laser-induced fluorescence (LIF).

In recent years, DME has become almost as popular secondary fuel component in NH_3 combustion research as H_2 or CH_4, due to DME being also considered an alternative fuel. Flames of NH_3/DME have been studied in terms of laminar burning velocity at room and elevated pressures (up to 5 atm) using air [21–23] or O_2/CO_2 [24] oxidizer, and with addition of H_2 to the NH_3/DME fuel mixture [25]. In addition to that, explosion characteristics of NH_3/DME have been studied with spark-ignited flames [26,27], and extinction strain rate of counterflow

* Corresponding author.
E-mail address: elna.heimdal_nilsson@fysik.lu.se (E.J.K. Nilsson).

https://doi.org/10.1016/j.fuel.2024.131951
Received 1 February 2024; Received in revised form 6 May 2024; Accepted 15 May 2024
Available online 24 May 2024

diffusion flames has been measured [28]. However, compared to NH_3/H_2 or NH_3/CH_4 (see above), NH_3/DME fuel mixture has been rarely characterized in terms of flame emissions or flame structure. Apart from turbulent swirl-flame diagnostics study of Lian et al. [29], only Yu et al. [13] has measured emissions from axisymmetric laminar flames, however, these measurements were not spatially resolved, as they were performed at the exhaust of the combustion chamber.

Reaction pathways of NO production for NH_3-containing fuels differ from pure hydrocarbons. While for the latter case, N_2 is the source of nitrogen atoms for NO, in practical fuel mixtures with NH_3, the ammonia mechanism dominates NO production. The NH_3-related chemistry has been extensively studied experimentally and theoretically (as reviewed in [30]), however, as described above, there is still a lack of spatially resolved experimental flame structure data for NH_3-containing binary fuels, that can serve as source for studies of reaction kinetics. Interpreting the experimentally measured NO concentrations in flames of NH_3/H_2 and NH_3/CH_4, Costa and co-workers [8,10] concluded that the primary effect of the second fuel component is limited to "reactions that regulate the temperature and amount of very reactive radicals, namely, O and OH", at the same time observing only a very limited influence of direct chemical interactions. Similar conclusions have been reached by Meng et al. [31] who studied NO formation in NH_3/DME flames with detailed kinetic modeling.

Considering the above, the present study has had two primary objectives: to investigate experimentally NO formation for a binary fuel mixture, of NH_3 and DME, extending the range of available flame structure data for practical NH_3-containing fuels, and to further analyze how NO formation chemistry is affected by DME. Distributions of NO were measured with 2D planar LIF (PLIF) in flames stabilized on a Bunsen-type burner at atmospheric pressure. The NH_3 content was varied from 10 % to 70 % (by mole) in the fuel mixture. The results were analyzed in terms of the kinetics of NO formation using several contemporary detailed reaction mechanisms [21,32–35], including analysis of the effect of carbon–nitrogen interactions on NO.

2. Experimental

The burner system, the laser diagnostics setup, and the NO quantification procedure are similar to what has been described in a previous work [20], which also include information related to uncertainty quantification, and only the most relevant information is summarized in this section. The burner is a stainless-steel metal tube with an inner diameter of 7 mm and a thickness of 1.5 mm. It is surrounded by a 50-mm outer tube with a clearance of 20 mm. The burner system is placed into a 25L stainless steel chamber with the exhaust ports located in the upper part of the chamber. A detailed description of the rig can be found in [36]. The NH_3/DME/air mixture was supplied through the inner tube, while co-flow air was fed into the outer tube. The measurements were conducted at atmospheric pressure. Before mixing with air, the NH_3/DME mixture was kept preheated to avoid condensation. The equivalence ratio (ϕ) varied from 0.9 to 1.2, and the fraction of NH_3 in the fuel mixture was 10–50 % at $\phi = 0.9$, 10–60 % at $\phi = 1.0$ and 1.2, and 10–70 % at $\phi = 1.1$. Flame stability limited the applicable equivalence ratios and NH3 fractions. The total flow rate of the combustible mixture was varied in order to keep heights of the cone-shaped flames at around 12 mm. The flow rate of the co-flow was varied to have similar outer velocity as the fuel/air mixture.

The configuration of the PLIF system for NO concentration measurements is described in [20]. Measurements of NO were made by probing the $Q_2(26.5)$ transition in the (0–0) band of the $A^2\Sigma^+ - X^2\Pi$ electronic transition at 225.5 nm by frequency-tripling a 676.5-nm laser beam from a dye laser pumped by an Nd:YAG laser. The vertical laser sheet was positioned above the burner tube in its symmetry plane. The PLIF signal was collected perpendicularly to the laser sheet with a CCD camera. A long-pass filter was placed in front of the camera to suppress scattering at the laser wavelength and straylight. Fluorescence from 300 single shots was collected and averaged before quantification.

The fluorescence signal was recorded in the linear regime, and quantification of the LIF signals into NO number densities was performed with a procedure similar to that used in [20]. In order to obtain calibration coefficients that depend on detector efficiency and collection optics, 2D Rayleigh scattering measurements were performed in ambient air. For the calculation of the Boltzmann population fraction and collisional quenching rate, a temperature of 2000 K was assumed, as these quantities do not possess a strong temperature dependence in regions corresponding to locations of maximal NO concentrations. The total uncertainty of the NO mole fractions was estimated to be 31 % [20], and it contains contributions from uncertainties in the LIF signal, the laser spectral irradiance, calibration coefficients, temperature-dependent quantities described above, and also from the uncertainty associated with background subtraction. Fuel condensation was avoided by applying band heaters to the inlet tube supplying fuel to the burner. Due to this preheating, the actual temperature of the reactant mixture was somewhat higher than 298 K, a value that was assumed in the simulations. This temperature difference was estimated to be around 10–15 K. Radial distributions of NO number densities evaluated at HAB (height above the burner) 8 mm were used for analysis and comparison with kinetic modeling. The selected position was located to avoid influences on the flame and LIF signal from the burner as well as to avoid effects on the flame due to closeness to its tip. Fig. 1 shows an example flame and its NO PLIF signal with the location of the line where quantitative LIF profiles were retrieved.

3. Modeling details

In the present study, a comparison between experimental and simulation results is performed by considering maximal values of NO concentrations extracted from each flame condition. The reason for this is the following. As opposed to NO formed during combustion of pure hydrocarbon fuels, for experimental cases of the present study, i.e., mixtures containing at least 10 % NH_3, NO is not chemically produced in the post-flame zone but only in the reaction zone. Therefore, each profile can be characterized by its maximal value attained in the reaction zone, which is then either preserved in the post-flame zone or NO is consumed. At the same time, previous work on NH_3/CH_4 flames [20] has shown that as far as maximal values are concerned, the experimental cone-shaped flame geometry does not affect NO concentrations. There [20], 2D DNS simulations were performed (with the mechanism of Okafor et al. [37]), and the results were compared to 1D free-propagating flames. The authors concluded that flame stretch does not affect NO formation in the reaction zone at the analyzed height above the burner, which equals 2/3 of the flame height for both [20] and the present work. Due to this, kinetic analysis of the present work is performed with a 1D free-propagating flame reactor model.

The simulations were performed in ANSYS Chemkin [38,39], with mixture-averaged transport properties and thermal diffusion, and post-

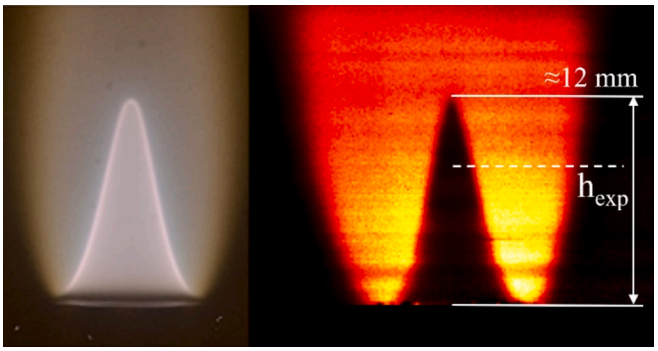

Fig. 1. Photo of the flame (left) and the corresponding NO PLIF image (right).

processing of the results was done using an in-house Python script. To model the experimental results of the present work, initial conditions of $T_u = 298$ K and p = 1 atm were assumed. The GRAD parameter was set to 2.5 %, corresponding to about 600–700 grid points in each solution. The experimentally determined radial distributions of NO number densities at 8 mm above the burner are recalculated into mole fractions using temperature profiles obtained from 1D simulations, positioned on the x-axis using half-maxima of the NO number densities.

3.1. Mechanism selection

There exist many mechanisms for NH3/DME combustion. For the present study, whose purpose is analysis of NO formation, detailed reaction schemes for NH_3/DME from three research groups have been selected, which do not share common submodels, in order to identify how much the difference in rate constants affects NO formation.

Dai et al. [32] studied NH_3/DME ignition chemistry and developed a detailed kinetic model in which the core chemistry subsets (C_1-C_2, H/N/O and C/H/N/O) were from the work of Glarborg et al. [30]. However, Glarborg [33] has since then published an updated version of the H/N/O detailed mechanism, which was later implemented in a detailed model for NH_3/n-heptane [40] with a new hydrogen sub-mechanism [41]. In this work, the NH_3/DME mechanism [32] was updated with new subsets [33,41], and in the following, this model will be referred to as "Glarborg 2022", and the original NH_3/DME mechanism of [32] as "Glarborg 2021".

Konnov and co-workers studied NO formation in neat DME flames and developed a detailed mechanism [42], the nitrogen sub-mechanism of which was first presented in [34]. Recently, an updated version of the mechanism in [34] was published [35], which was further validated in terms of NO formation during combustion and oxidation of neat NH_3 mixtures. Similarly, the NH_3/DME mechanism [42] and its updated version according to [35] will be referred to as "Konnov 2022" and "Konnov 2023", respectively.

Finally, Issayev et al. [21] developed a detailed NH_3/DME mechanism to represent the ignition and flame chemistry of these binary mixtures. This mechanism continues the work of Mauss and co-workers [43–45], from which it has received its different subsets.

4. Results

Fig. 2 shows the experimentally determined NO concentration for a flame of 40/60 NH_3/DME mixture (by mole) at $\phi = 1.1$ and modeling results calculated with the detailed mechanisms [21,32,33,35,42]. Both experiments and simulations indicate fast NO formation in the reaction zone, followed by a plateau region with a slow decrease in NO mole fraction in the post-flame region. The experimental NO profiles, however, tend to suggest a delayed attainment of maxima, compared to 1D simulations. A similar trend is clearly visible in results of the previous study [20], conducted with the same experimental procedure, and is therefore unrelated to the flame stretch being unaccounted for in the 1D modeling, as 2D DNS results in [20] agree with the free-propagating flame model. The 2D effects can, however, explain different rates of NO decrease in the post-flame zone (see Figs. 7-8 in [20]). Therefore, in the following, experiments and simulations are compared in terms of maximal NO concentrations for all flames. All experimental NO radial distributions are provided in the Supplementary Material (SM).

Fig. 3 shows maximal mole fractions of NO for flames with ϕ = 0.9–1.2 (Fig. 3 (a-d)) and varied amount of NH_3 in the initial NH_3/DME mixture (by mole), X_{NH3}. The experiments covered mixtures with X_{NH3} = 10–70 %, while simulations were performed for the whole range. For modeled cases with $X_{NH3} \to 0$, the term "maximal NO" corresponds to the reaction zone concentration, as NO is formed in post-flame.

The common trend followed by experiments and models is the sharp increase in NO formation for mixtures ranging from 10 % to 30 % NH_3 and for 40 %-60 % mixtures, experiments indicate nearly similar NO

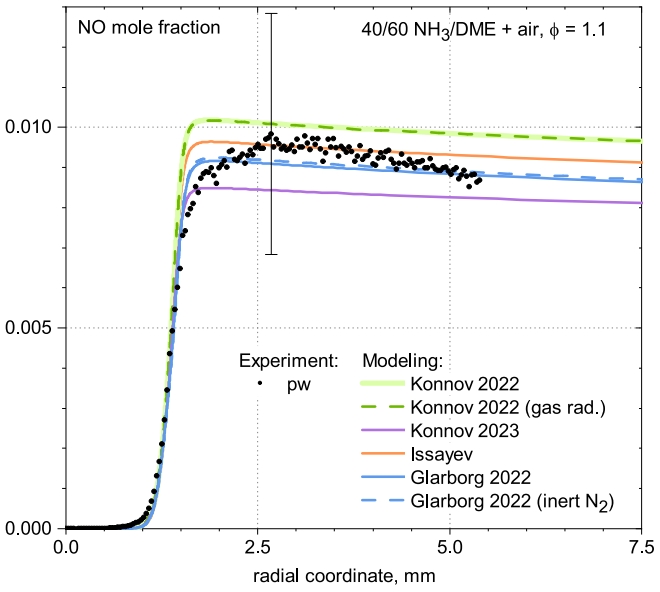

Fig. 2. Radial distribution of NO for a 40/60 NH_3/DME + air flame at $\phi = 1.1$ and HAB 8 mm measured in the present work (symbols) and simulated in 1D with models [21,32,33,35,42] (lines). Also illustrated are the effects of gas radiation (for [34] "gas rad.", green dashed) and of N_2 in air ("inert N_2" for [33], blue dashed). (For interpretation of the references to colour in this figure legend, the reader is referred to the web version of this article.)

concentrations, considering the uncertainty range, for mixtures with the same ϕ. The experimental results also hint that peak NO values from each panel of Fig. 3 decrease with increasing ϕ. This, however, can be clearly traced from the modeling results, also, the simulations suggest that the values of X_{NH3} at which these maxima are observed decrease with ϕ. Quantitatively, however, the X_{NH3} corresponding to maximum NO mole fraction differs between the investigated mechanisms.

All model predictions obtained with all mechanisms are within the experimental uncertainty range. Overall, it can be concluded that the updated "Glarborg 2022" and "Konnov 2023" mechanisms follow the experiments the best. However, while the difference in predictions between the two versions of the Glarborg mechanisms is minimal, the original "Konnov 2022" [42] deviates from the rest in lean and stoichiometric cases (Fig. 3 a,b), while at $\phi = 1.2$ the difference between the two versions of the Konnov model is smaller. This is as expected since modifications inside the Konnov model affected high-temperature chemistry [35], while updates in the Glarborg mechanism mainly concerned the intermediate temperature region. Finally, the mechanism of Issayev et al. [21] generally predicts slightly higher NO concentrations than "Konnov 2023" and "Glarborg 2022", and except for the stoichiometric case (Fig. 3b), follows the experimental results to the same level of accuracy as the former two mechanisms.

It can be noticed from Fig. 3 that outside the experimentally investigated range, i.e. at $X_{NH3} < 10$ %, and $X_{NH3} > 70$ %, all model predictions are in closer agreement with each other (aside from "Konnov 2022" [42] at $\phi \leq 1$; $X_{NH3} > 70$ %). However, while NO formation in 100 % NH_3 mixtures is of the same order of magnitude as for X_{NH3} = 10–70 %, in neat DME flames, it is practically absent compared to NH_3-containing fuel mixtures. To further assess model predictions at these conditions, Figs. 4 and 5 present experimental results from literature for DME/air flames [42] and for a stoichiometric NH_3/O_2/Ar flame [17]. The former data have been used in the development of the "Konnov 2022" model [42], while the results of Osipova et al. [17] served as one of the validation targets for the "Konnov 2023" model[35].

Out of the mechanisms considered in the present work, the model of Issayev et al. is in best quantitative agreement with experiments [17] for the 100 % NH_3 flame (Fig. 5), followed by the updated "Konnov 2023"

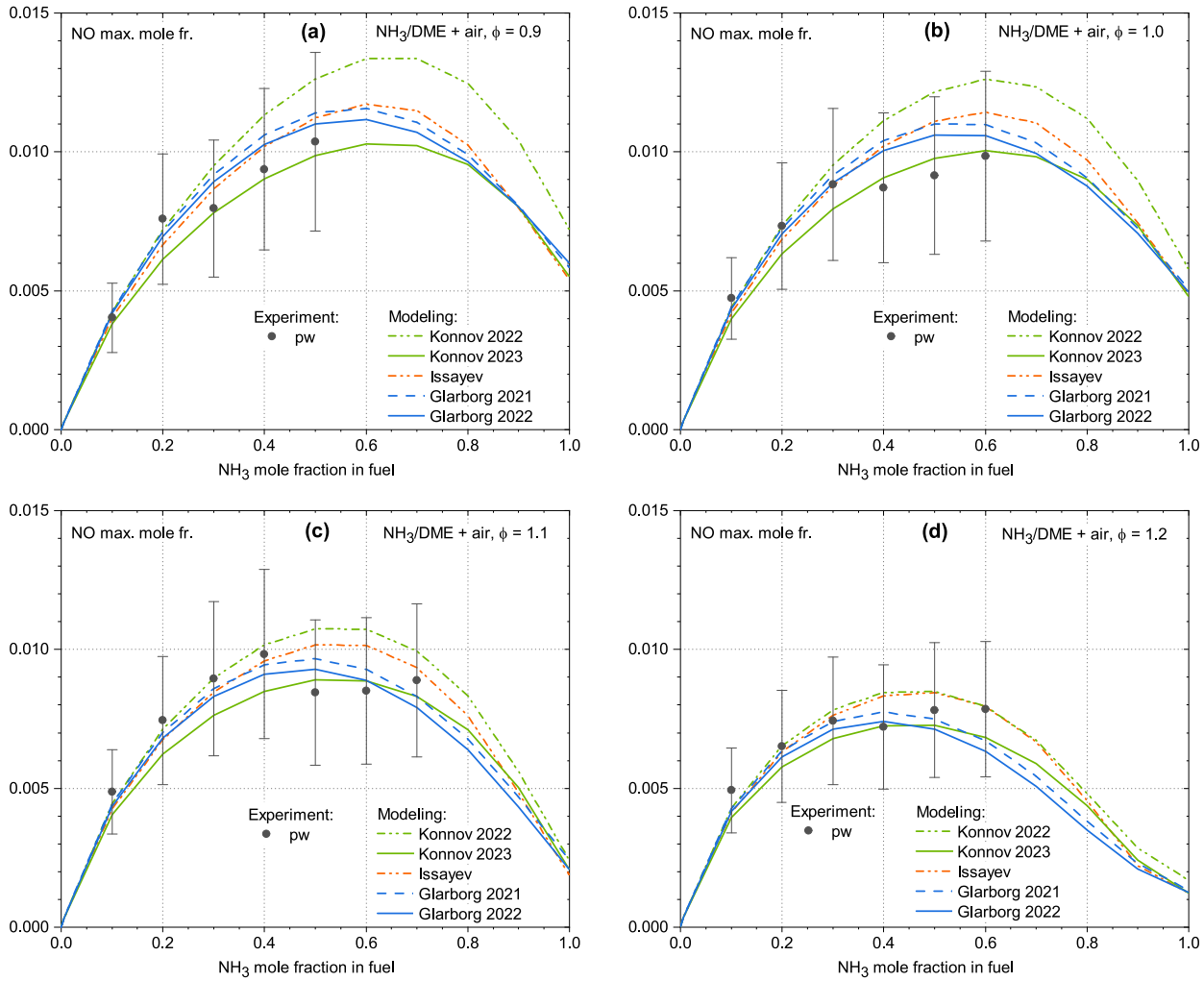

Fig. 3. Maximal NO concentrations vs. initial NH_3 mole fraction in the fuel mixture for flames with $\phi = 0.9$–1.2 (a-d), obtained from the experimental radial NO distributions (symbols) and from 1D simulations using models [21,32,33,35,42] (lines).

and "Glarborg 2022" models. The situation is different for neat DME flames (Fig. 4), where the two versions of the Konnov mechanism are closest to experiments [42]. Note that this is the only mechanism that provides gas radiation coefficients, and in Fig. 4, results with (solid green line) and without gas radiation (dashed and dash-dot green lines) are presented for the Konnov mechanisms for a fair comparison with the rest. It can be seen, however, that while the radiation effect is visible, especially for near-stoichiometric mixtures, the predictions of the Glarborg mechanisms and that of Issayev et al. would still be outside the experimental error bars even with radiation considered.

Fig. 4 also serves to visualize that while accounting for radiation can affect the prediction of NO_x in the combustion of hydrocarbon fuels, it can be safely disregarded for NH_3-containing mixtures, see Fig. 2, in which the NO profile is additionally calculated with model [42] with and without gas radiation. In addition to that, the kinetic effect of N_2 in air, which results in the formation of thermal NO for hydrocarbon fuels, is illustrated for NH_3-containing mixtures. Additional modeling was performed with a modified Glarborg mechanism, in which N_2 from air was able to participate in elementary reactions as a third-body only (dashed blue line in Fig. 2). It can be concluded that the kinetic effect of N_2 in air can be disregarded as well.

5. Analysis

Fig. 3 indicates that the Glarborg 2022 [32,33], Konnov 2023 [35,42] and Issayev et al. [21] mechanisms do not deviate from each other dramatically, with the differences between the predictions being less or around 25 % of the experimental uncertainty interval. Further analysis has shown that kinetic differences in the nitrogen sub-mechanisms are mainly limited to values of rate constants of several key reactions. However, the effect of the direct chemical coupling was the most pronounced for the Glarborg model, as discussed below. Considering these, in the following section, the reaction kinetics of NO formation will be illustrated with the Glarborg 2022 model, and the key differences compared with the other models will be then outlined.

Fig. 6 presents the sensitivity analysis for the maximal NO concentration in flames with 10, 50 and 90 % NH_3 and $\phi = 0.9$, 1.1, calculated with the Glarborg 2022 mechanism [32,33]. First of all, reactions in the top 25 charts almost exclusively originate from the H/N/O subset. Going from 10 % to 50 % NH_3, NO production increases (see Fig. 3) due to the increasing amount of NH_3, and so does the sensitivity of all major reactions. Then, with a further increase of NH_3 and decrease of DME in the initial mixture, relative concentrations of radicals in the radical pool of O, H, and OH start to change. It can be exemplified by looking at the sensitivity of reactions involving the O atom:

$$NH + O = NO + H \quad \text{(R1)}$$

$$NH_2 + O = HNO + H \quad \text{(R2)}$$

which decreases for 90 % NH_3 mixtures compared to 50 % NH_3,

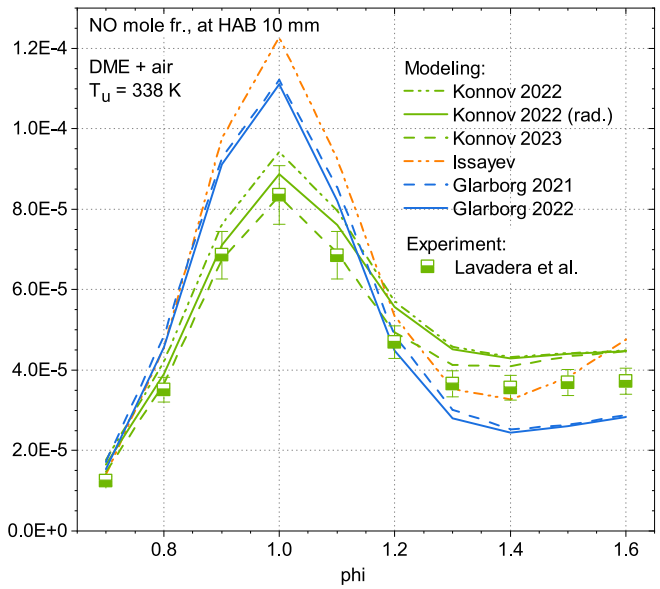

Fig. 4. NO mole fractions at HAB = 10 mm for adiabatic DME + air flames measured by Lubrano Lavadera et al. [42] and simulated with models [21,32,33,35,42] (lines). Predictions of [42] are additionally simulated with radiative heat losses (solid green line). (For interpretation of the references to colour in this figure legend, the reader is referred to the web version of this article.)

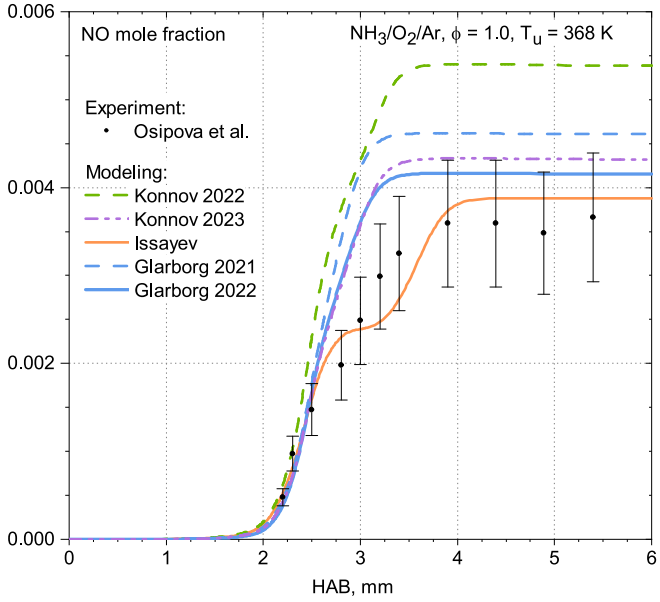

Fig. 5. Profile of NO for stoichiometric $NH_3/O_2/Ar$ flame at 368 K, measured experimentally by Osipova et al. [17] (symbols) and simulated using mechanisms [21,32,33,35,42] (lines). Modeling was performed using the experimental temperature profile reported in [17].

since, as known for NH_3 flames (see, e.g. [23,46]), the amount of O-radical compared to OH is lower in flames with high NH_3 content. On the other hand, in these mixtures, reactions of HNO, a main intermediate in NH_3 oxidation, e.g.:

$$NH + OH = HNO + H \quad (R3)$$

$$NO + H(+M) = HNO(+M) \quad (R4)$$

$$NHO + H = NO + H2 \quad (R5)$$

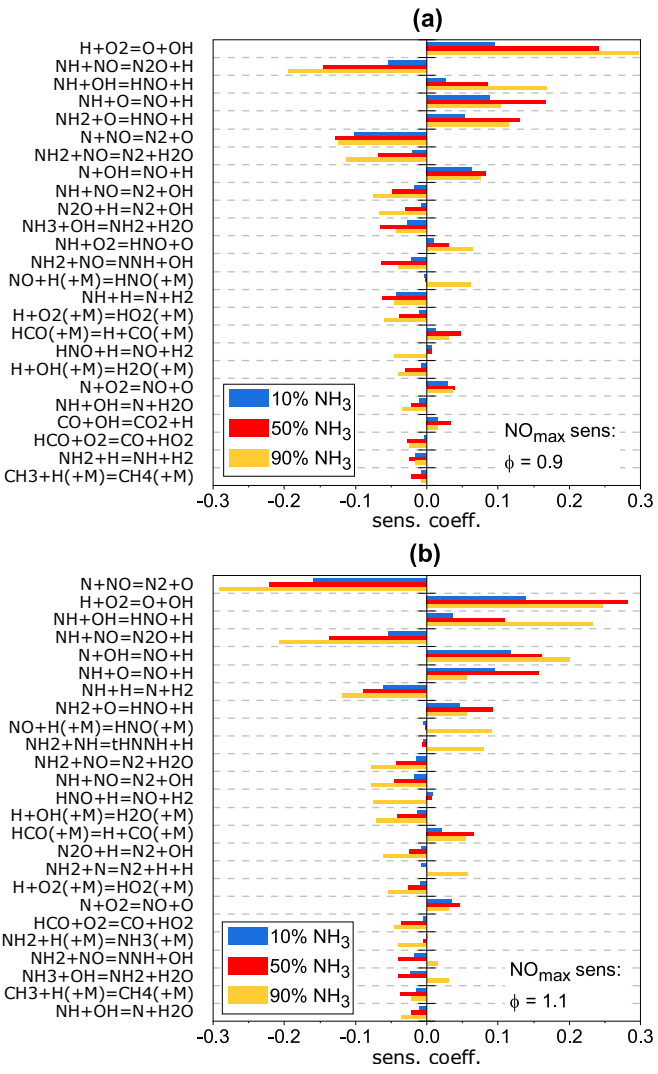

Fig. 6. Sensitivity of the maximal NO concentrations to elementary reactions of the Glarborg 2022 mechanism [32,33] for NH_3/DME flames with $\phi = 0.9$ (a), $\phi = 1.1$ (b) and with 10,50 or 90 % NH_3 (by mole) in the fuel.

become very important. Note the large negative sensitivity of (R5) for 90 % mixtures, despite the fact that it leads to the production of NO. This is because (R5) is also, and more importantly, a termination reaction that affects overall NH_3 chemistry (as discussed by e.g. Okafor et al. [47]).

Lower temperatures and lower radical concentration supress formation of NO, an explanation to why NO decrease as NH_3 content in flames approach 100 %. Such behavior of NO concentrations against NH_3 percentage in the fuel mixture is universal and has been observed in kinetic studies for various NH_3 binary fuels: NH_3/CH_4 ([48], syngas and H_2 [46]) and in the experimental study of NO emissions from NH_3/DME flames [13].

Considering reactions hindering NO formation, variation of the NH_3 content changes the relative importance of the two main NO consumption channels in the reaction zone, i.e.:

$$NH + NO = N_2O + H \quad (R6)$$

$$N + NO = N2 + O \quad (R7)$$

This is due to changes in relative concentrations of NH and N in flames with different initial NH_3 content. Further rate of production analysis indicated that the production of N from NH has a significantly larger selectivity for low NH_3 content mixtures, specifically due to

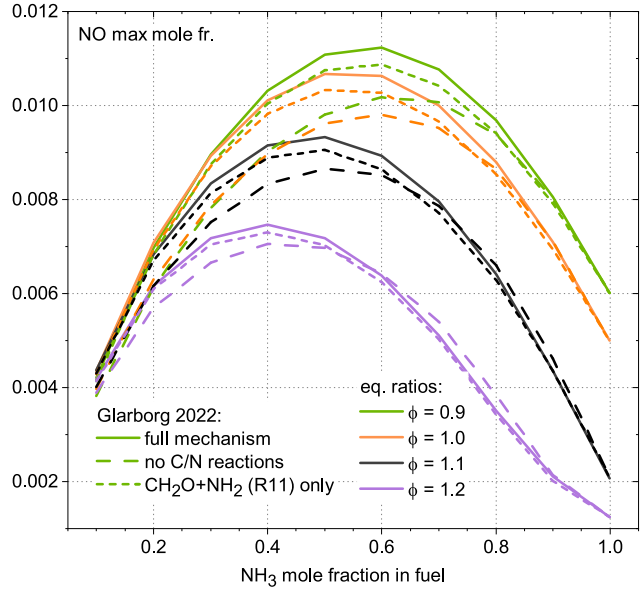

Fig. 7. Effect of the C/N interactions on NO formation, analyzed with the Glarborg 2022 model [32,33]. Solid lines: full mechanism, long dash: mechanism without C/N reactions, short dash: no interactions, except for a single reaction $CH_2O + NH_2 = HCO + NH_3$ (R11).

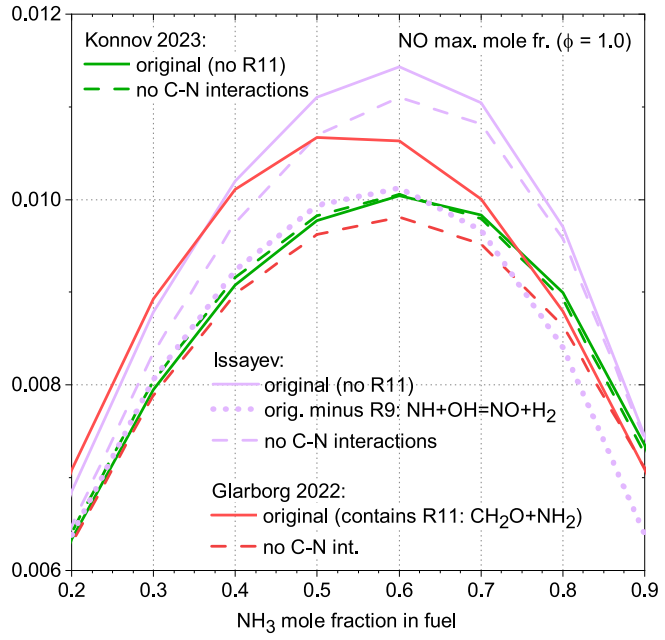

Fig. 8. Effect of the C/N interactions on NO formation, analyzed for NH_3/DME mixtures at $\phi = 1.0$ with three models: Glarborg 2022 [32,33] (red), Konnov 2023 [35,42] (green), and Issayev et al. [21] (violet). Solid lines: original mechanisms, dashed lines: mechanisms without C/N reactions; dotted line: (For interpretation of the references to colour in this figure legend, the reader is referred to the web version of this article.)

radical–radical reaction

$$NH_2 + NH = HNNH + H \quad (R8)$$

that becomes possible only when the amount of NH_3, and consequently, NH_2 and NH radicals, is high. Overall, the two main trends for mixtures with increasing NH_3 fraction are: a) for NO formation, the sensitivity of O-atom reactions, such as (R1) and (R2), decreases, while that of OH reactions, such as (R3), increases, due to changes in the radical pool, and b) for NO consumption, reaction R(6) becomes as important as (R7).

Note that the sensitivity of O-atom reactions remains high even in 90 % NH_3 mixtures. This has been discussed by Chen et al. [35], who proposed modification of (R2) in the Konnov 2022 model [42], and it has been identified as the main reason for the improved NO prediction in neat NH_3 flames (see [35] or Fig. 5 which contains one of their validation cases). This trend is preserved in binary NH_3-containing mixtures as well. As the rate constant in the Konnov model was replaced with the same expression as in the Glarborg mechanism, the predictions of the two mechanisms become much closer (see Fig. 3), and the sensitivity spectra for the Konnov 2023 model [35] are similar to ones presented in Fig. 6.

The mechanism of Issayev et al. [21] has different (by about a factor of ~ 2–3) values of rate constants of many key reactions discussed above, but most notably, contains another branch channel of (R3), i.e.

$$NH + OH = NO + H2 \quad (R9)$$

with a rate similar to (R3). Reaction channel (R9) is absent in the Glarborg mechanism, and in the Konnov model, it has a significantly lower branching ratio compared to (R3). Klippenstein et al. [49] have very recently revisited the NH + OH reaction. However, their calculated rate expressions for (R3) and the third channel.

$$NH + OH = N + H_2O(R \quad 10)$$

turned out to be close to the values from their earlier work [50], utilized in the Glarborg mechanism, while the calculated branching ratio between (R3) and (R9) from [49] is 80/20. Without the channel (R9), the mechanism of Issayev et al. [21] gives predictions very close to Konnov 2023, and the remaining difference between Glarborg 2022 and Konnov 2023 is due to direct chemical interactions between carbon- and nitrogen-containing species, which is discussed in detail below.

The sensitivity spectra of Fig. 6 do not contain any reactions between carbon- and nitrogen-containing species. It is known that direct chemical interactions play an important role in the ignition chemistry of NH_3-containing mixtures [21,32,40,51], but can be disregarded for laminar burning velocity [52]. In order to illustrate the degree of importance of the interaction reactions for the formation of NO in flames of NH_3/DME, simulations were first performed with the Glarborg 2022 mechanism [32,33]. A modified version was constructed, from which all reactions between carbon- and nitrogen-containing species have been deleted. Maximal NO concentrations for NH_3/DME mixtures with $\phi = 0.9$–1.2 and $X_{NH3} \geq 10$ % are presented in Fig. 7. Without C-N reactions, the peak values of the maximal NO concentrations at each ϕ decrease by 5–9 %, higher for leaner mixtures. The positions of the peaks shift to mixtures with higher NH_3 mole fraction by about 0.05, e.g., from $X_{NH3} \approx 0.55$ to $X_{NH3} \approx 0.6$ if C-N reactions are not considered. Further analysis has shown that, to a large extent, the difference is due to the presence of a single reaction:

$$CH_2O + NH_2 = HCO + NH_3(R \quad 11)$$

As shown in Fig. 7, if the whole C-N submechanism of the Glarborg model contains only (R11), its predictions become very close to the full mechanism. While the rate of production analysis has shown that (R11) does contribute significantly to the conversion of CH_2O to HCO, the effect of (R11) on NO formation comes from NH_3 recombination. Due to this, NH_3 starts to be present further down in the flame, resulting in chain reactions of the NH_3 sub-mechanism occurring at higher temperatures, and this increases NO concentration. The combined influence of all other reactions from the C/H/N/O subset is still noticeable in Fig. 7. However, it is (R11) that determines positions on the x-axis, at which NO concentration maxima are observed.

There are two recent studies [24,53] that question the rate constant of (R11) in the Glarborg mechanism. Specifically, Shi et al. [24] found disagreement in the rate expression with its source study [54], and

provided new calculated value for R11, that was found to be in agreement with the value suggested in the PSR study of Zhu et al. [53], who obtained R11 by fitting the simulated NH_3 consumption profile to the experimental data. The rate constant from [24,53] is more than an order of magnitude smaller than in the Glarborg model, making its influence on NO formation effectively negligible.

Similar calculations as in Fig. 7 have been performed with the Konnov 2023 [35,42] and Issayev et al. [21] mechanisms for stoichiometric NH_3/DME mixtures with and without C-N subsets (Fig. 8). These mechanisms do not contain (R11), and for this reason, the difference between the predictions of the mechanisms with and without the C/H/N/O subset is smaller compared to the Glarborg mechanism, especially for the Konnov model. Note that predictions of the Konnov model (either with or without C/H/N/O) are very close to the Glarborg mechanism without interactions. Note also that in Fig. 5, which concerns NO formation in a neat NH_3 flame, predictions of the Glarborg and Konnov 2023 models are very close, and the difference to Konnov 2022 is due to (R2) as discussed in [35]. Therefore, these two mechanisms can be considered very similar in terms of NO formation in NH_3/DME flames, provided (R2) has an updated value (see [35]) and that R(11) in overestimated in the Glarborg mechanism… The predictions of the Issayev et al. mechanism without (R9), whose rate constant is likely overestimated as discussed above, are also shown in Fig. 8 (violet dotted line). Its predictions became closer to the other mechanisms, however, note that in Issayev et al., reaction (R2) is still around a factor of 3 faster than in Glarborg 2022 and Konnov 2023. Overall, selection of rate constants for reactions (R(2), R9, R11) noticeably affects NO formation in NH_3/DME flames. *Issayev et al.* [21] *without R9:* $NH + OH = NO + H_2$.

The analysis of this section also has practical implications in terms of developing reduced reaction schemes for NH_3 binary fuels, which can be used for simulations of real combustors and are required to reproduce NO emissions. If such a scheme is obtained by mechanism merging, then the hydrocarbon subset has to predict correct levels of H, O and OH radicals to be coupled with a NH_3 sub-mechanism. At the same time, a direct chemical coupling can to a large extent be excluded.

6. Conclusions

In the present work, the formation of nitric oxide has been studied in flames of mixtures of ammonia and DME with varying equivalence ratios ($\phi = 0.9$–1.2) and composition (10–50 % NH_3 in the fuel mixture at $\phi =$ 0.9, 10–60 % at $\phi = 1.0$ and 1.2, and 10–70 % at $\phi = 1.1$). Laminar flames have been stabilized on a Bunsen-type burner, and 2D-PLIF has been implemented to perform quantitative measurements of NO.

Following the analysis of the experimental and modeling results, it was concluded that in the studied range of initial mixture parameters, NO formation decreases with an increasing equivalence ratio. By increasing the fraction of NH_3 in the fuel mixture, NO formation first increases, peaks at a certain percentage, and then goes down with a further increase in NH_3 content. The values of the NH_3 fraction at which NO emissions reach maximum are equivalence-ratio-dependent. Overall, emissions of NO for NH_3/DME fuel can reach up to 1 % in the product gas, and these emissions are maximal for mixtures with 40–60 % NH_3.

Kinetic analysis has shown that chemical pathways for NO formation originate solely in the NH_3 submechanism. The importance of the hydrocarbon fuel chemistry is that it affects the overall heat release and the amount and fraction of radicals of the hydrogen submechanism. As for interaction reactions, a particular effect of the H-abstraction reaction from formaldehyde by HN_2 (R11) on maximal NO concentrations was observed. It has also been found that the difference in the performance of contemporary NH_3/DME mechanisms from three research groups [21,32,33,35,42] differ due to either absence or variations in the rate expressions of different reactions. Of a particular notice are three reactions: (R2), (R9), (R11). Overall, however, all observed differences were found to be less than the experimental uncertainty.

The observed results in terms of direct chemical interactions have practical implications for the development of reduced reaction schemes for practical combustors: to correctly predict NO emissions from flames, the interaction chemistry can be largely disregarded.

CRediT authorship contribution statement

Vladimir A. Alekseev: Writing – original draft, Validation, Methodology, Formal analysis, Data curation, Conceptualization. **Christian Brackmann:** Writing – review & editing, Methodology, Investigation, Formal analysis, Data curation, Conceptualization. **Xin Liu:** Investigation. **Elna J.K. Nilsson:** Writing – review & editing, Supervision, Project administration, Funding acquisition, Formal analysis.

Declaration of competing interest

The authors declare that they have no known competing financial interests or personal relationships that could have appeared to influence the work reported in this paper.

Data availability

Data will be made available on request.

Acknowledgements

VA and EN would like to acknowledge that their contribution is part of the project ENGIMMONIA, which has received funding from the European Research Council (ERC) under the European Union's Horizon 2020 research and innovation program (Grant agreement No. 955413). CB would like to acknowledge funding from the Swedish Energy Agency through (Competence Center CECOST, 22538-4).

Appendix A. Supplementary data

Supplementary data to this article can be found online at https://doi.org/10.1016/j.fuel.2024.131951.

References

[1] Chiong M-C, Chong CT, Ng J-H, Mashruk S, Chong WWF, Samiran NA, et al. Advancements of combustion technologies in the ammonia-fuelled engines. Energ Conver Manage 2021;244:114460. https://doi.org/10.1016/j.enconman.2021.114460.
[2] Jin S, Wu B, Zi Z, Yang P, Shi T, Zhang J. Effects of fuel injection strategy and ammonia energy ratio on combustion and emissions of ammonia-diesel dual-fuel engine. Fuel 2023;341:127668. https://doi.org/10.1016/j.fuel.2023.127668.
[3] Zhang Z, Long W, Dong P, Tian H, Tian J, Li B, et al. Performance characteristics of a two-stroke low speed engine applying ammonia/diesel dual direct injection strategy. Fuel 2023;332:126086. https://doi.org/10.1016/j.fuel.2022.126086.
[4] Førby N, Thomsen TB, Cordtz RF, Bræstrup F, Schramm J. Ignition and combustion study of premixed ammonia using GDI pilot injection in CI engine. Fuel 2023;331:125768. https://doi.org/10.1016/j.fuel.2022.125768.
[5] Gross CW, Kong S-C. Performance characteristics of a compression-ignition engine using direct-injection ammonia–DME mixtures. Fuel 2013;103:1069–79. https://doi.org/10.1016/j.fuel.2012.08.026.
[6] Ryu K, Zacharakis-Jutz GE, Kong S-C. Performance characteristics of compression-ignition engine using high concentration of ammonia mixed with dimethyl ether. Appl Energy 2014;113:488–99. https://doi.org/10.1016/j.apenergy.2013.07.065.
[7] Niki Y. Reductions in Unburned Ammonia and Nitrous Oxide Emissions From an Ammonia-Assisted Diesel Engine With Early Timing Diesel Pilot Injection. J Eng Gas Turbines Power 2021;143. https://doi.org/10.1115/1.4051002.
[8] Rocha RC, Ramos CF, Costa M, Bai X-S. Combustion of NH3/CH4/Air and NH3/H2/Air Mixtures in a Porous Burner: Experiments and Kinetic Modeling. Energy Fuel 2019;33:12767–80. https://doi.org/10.1021/acs.energyfuels.9b02948.
[9] Joo JM, Lee S, Kwon OC. Effects of ammonia substitution on combustion stability limits and NOx emissions of premixed hydrogen–air flames. Int J Hydrogen Energy 2012;37:6933–41. https://doi.org/10.1016/j.ijhydene.2012.01.059.
[10] Filipe Ramos C, Rocha RC, Oliveira PMR, Costa M, Bai X-S. Experimental and kinetic modelling investigation on NO, CO and NH3 emissions from NH3/CH4/air premixed flames. Fuel 2019;254:115693. https://doi.org/10.1016/j.fuel.2019.115693.
[11] Weng W, Li S, Aldén M, Li Z. Ultraviolet Absorption Cross-Sections of Ammonia at Elevated Temperatures for Nonintrusive Quantitative Detection in Combustion

Environments. Appl Spectrosc 2021;75:1168–77. https://doi.org/10.1177/0003702821990445.
[12] Jójka J, Ślefarski R. Dimensionally reduced modeling of nitric oxide formation for premixed methane-air flames with ammonia content. Fuel 2018;217:98–105. https://doi.org/10.1016/j.fuel.2017.12.070.
[13] Yu M, Luo G, Sun R, Qiu W, Chen L, Wang L, et al. Experimental and numerical study on emission characteristics of NH3/DME/air flames in a premixed burner. Combust Flame 2024;259:113098. https://doi.org/10.1016/j.combustflame.2023.113098.
[14] Henshaw PF, D'Andrea T, Mann KRC, Ting DSK. Premixed Ammonia-Methane-Air Combustion. Combust Sci Technol 2005;177:2151–70. https://doi.org/10.1080/00102200500240695.
[15] C. Duynslaegher, H. Jeanmart,J. Vandooren, Flame structure studies of premixed ammonia/hydrogen/oxygen/argon flames: Experimental and numerical investigation, Proceedings of the Combustion Institute 2009; 32: 1277-1284, Doi: 10.1016/j.proci.2008.06.036.
[16] Tian Z, Li Y, Zhang L, Glarborg P, Qi F. An experimental and kinetic modeling study of premixed NH3/CH4/O2/Ar flames at low pressure. Combust Flame 2009;156:1413–26. https://doi.org/10.1016/j.combustflame.2009.03.005.
[17] Osipova KN, Korobeinichev OP, Shmakov AG. Chemical structure and laminar burning velocity of atmospheric pressure premixed ammonia/hydrogen flames. Int J Hydrogen Energy 2021;46:39942–54. https://doi.org/10.1016/j.ijhydene.2021.09.188.
[18] Osipova KN, Sarathy SM, Korobeinichev OP, Shmakov AG. Chemical structure of premixed ammonia/hydrogen flames at elevated pressures. Combust Flame 2022;246:112419. https://doi.org/10.1016/j.combustflame.2022.112419.
[19] Yang X, Peng Z, Ding Y, Du Y. Spatially resolved broadband absorption spectroscopy measurements of temperature and multiple species (NH, OH, NO, and NH3) in atmospheric-pressure premixed ammonia/methane/air flames. Fuel 2023;332:126073. https://doi.org/10.1016/j.fuel.2022.126073.
[20] Rocha RC, Zhong S, Xu L, Bai X-S, Costa M, Cai X, et al. Structure and Laminar Flame Speed of an Ammonia/Methane/Air Premixed Flame under Varying Pressure and Equivalence Ratio. Energy Fuel 2021;35:7179–92. https://doi.org/10.1021/acs.energyfuels.0c03520.
[21] Issayev G, Giri BR, Elbaz AM, Shrestha KP, Mauss F, Roberts WL, et al. Ignition delay time and laminar flame speed measurements of ammonia blended with dimethyl ether: A promising low carbon fuel blend. Renew Energy 2022;181:1353–70. https://doi.org/10.1016/j.renene.2021.09.117.
[22] Xiao H, Li H. Experimental and kinetic modeling study of the laminar burning velocity of NH3/DME/air premixed flames. Combust Flame 2022;245:112372. https://doi.org/10.1016/j.combustflame.2022.112372.
[23] Yin G, Li J, Zhou M, Li J, Wang C, Hu E, et al. Experimental and kinetic study on laminar flame speeds of ammonia/dimethyl ether/air under high temperature and elevated pressure. Combust Flame 2022;238:111915. https://doi.org/10.1016/j.combustflame.2021.111915.
[24] Shi X, Li W, Zhang J, Fang Q, Zhang Y, Xi Z, et al. Exploration of NH3 and NH3/DME laminar flame propagation in O2/CO2 atmosphere: Insights into NH3/CO2 interactions. Combust Flame 2024;260:113245. https://doi.org/10.1016/j.combustflame.2023.113245.
[25] Li H, Xiao H. Effect of H2 addition on laminar burning velocity of NH3/DME blends by experimental and numerical method using a reduced mechanism. Combust Flame 2023;257:113000. https://doi.org/10.1016/j.combustflame.2023.113000.
[26] Zhang Z, Zheng K, Ning X, Wang X, Wang J. Study on Explosion Characteristics of Ammonia/Dimethyl Ether/Air with Different Mixed Compositions. Energy Fuel 2023;37:11270–83. https://doi.org/10.1021/acs.energyfuels.3c01551.
[27] Li H, Xiao H. Experimental study on the explosion characteristics of NH3/DME/air mixtures. Fuel 2023;352:129069. https://doi.org/10.1016/j.fuel.2023.129069.
[28] Chen J, Gou X. Experimental and kinetic study on the extinction characteristics of ammonia-dimethyl ether diffusion flame. Fuel 2023;334:126743. https://doi.org/10.1016/j.fuel.2022.126743.
[29] Lian T, Shi X, Han S, Zhang Y, Liu Z, Xi Z, et al. Unraveling the impact of CO2 exhaust gas recirculation on flame characteristics and NOx emissions of premixed NH3/DME swirl flames. Applications in Energy and Combustion Science 2024;17:100256. https://doi.org/10.1016/j.jaecs.2024.100256.
[30] Glarborg P, Miller JA, Ruscic B, Klippenstein SJ. Modeling nitrogen chemistry in combustion. Prog Energy Combust Sci 2018;67:31–68. https://doi.org/10.1016/j.pecs.2018.01.002.
[31] Meng X, Zhang M, Zhao C, Tian H, Tian J, Long W, et al. Study of combustion and NO chemical reaction mechanism in ammonia blended with DME. Fuel 2022;319:123832. https://doi.org/10.1016/j.fuel.2022.123832.
[32] Dai LM, Hashemi H, Glarborg P, Gersen S, Marshall P, Mokhov A, et al. Ignition delay times of NH3/DME blends at high pressure and low DME fraction: RCM experiments and simulations. Combust Flame 2021;227:120–34. https://doi.org/10.1016/j.combustflame.2020.12.048.
[33] Glarborg P. The NH3/NO2/O2 system: Constraining key steps in ammonia ignition and N2O formation. Combust Flame 2023;257:112311. https://doi.org/10.1016/j.combustflame.2022.112311.
[34] Han X, Lubrano Lavadera M, Konnov AA. An experimental and kinetic modeling study on the laminar burning velocity of NH3+N2O+air flames. Combust Flame 2021;228:13–28. https://doi.org/10.1016/j.combustflame.2021.01.027.
[35] Chen J, Lubrano Lavadera M, Konnov AA. An experimental and modeling study on the laminar burning velocities of ammonia+oxygen+argon mixtures. Combust Flame 2023;255:112930. https://doi.org/10.1016/j.combustflame.2023.112930.
[36] Joo PH, Gao J, Li Z, Aldén M. Experimental apparatus with full optical access for combustion experiments with laminar flames from a single circular nozzle at elevated pressures. Rev Sci Instrum 2015;86:035115. https://doi.org/10.1063/1.4915624.
[37] Okafor EC, Naito Y, Colson S, Ichikawa A, Kudo T, Hayakawa A, et al. Measurement and modelling of the laminar burning velocity of methane-ammonia-air flames at high pressures using a reduced reaction mechanism. Combust Flame 2019;204:162–75. https://doi.org/10.1016/j.combustflame.2019.03.008.
[38] ANSYS Chemkin 2020 R2. 2020, ANSYS, Inc.
[39] ANSYS Chemkin 17.0 15151. 2015, ANSYS, Inc.
[40] Thorsen LS, Jensen MST, Pullich MS, Christensen JM, Hashemi H, Glarborg P, et al. High pressure oxidation of NH3/n-heptane mixtures. Combust Flame 2023;254:112785. https://doi.org/10.1016/j.combustflame.2023.112785.
[41] H. Zhao, C. Yan, Z. Wang, A.W. Jasper, S.J. Klippenstein,Y. Ju, High-pressure hydrogen oxidation in N2, CO2, and H2O dilutions up to 100 atm in a supercritical-pressure jet-stirred reactor, In preparation 2022.
[42] Lubrano Lavadera M, Brackmann C, Konnov AA. Laminar burning velocities and nitric oxide formation in premixed dimethyl ether/air flames: Experiments and kinetic modeling. Combust Flame 2022;246:112411. https://doi.org/10.1016/j.combustflame.2022.112411.
[43] Shrestha KP, Eckart S, Elbaz AM, Giri BR, Fritsche C, Seidel L, et al. A comprehensive kinetic model for dimethyl ether and dimethoxymethane oxidation and NOx interaction utilizing experimental laminar flame speed measurements at elevated pressure and temperature. Combust Flame 2020;218:57–74. https://doi.org/10.1016/j.combustflame.2020.04.016.
[44] Shrestha KP, Seidel L, Zeuch T, Mauss F. Detailed Kinetic Mechanism for the Oxidation of Ammonia Including the Formation and Reduction of Nitrogen Oxides. Energy Fuel 2018;32:10202–17. https://doi.org/10.1021/acs.energyfuels.8b01056.
[45] Shrestha KP, Seidel L, Zeuch T, Mauss F. Kinetic Modeling of NOx Formation and Consumption during Methanol and Ethanol Oxidation. Combust Sci Technol 2019;191:1627–59. https://doi.org/10.1080/00102202.2019.1606804.
[46] Wang S, Wang Z, Elbaz AM, Han X, He Y, Costa M, et al. Experimental study and kinetic analysis of the laminar burning velocity of NH3/syngas/air, NH3/CO/air and NH3/H2/air premixed flames at elevated pressures. Combust Flame 2020;221:270–87. https://doi.org/10.1016/j.combustflame.2020.08.004.
[47] Okafor EC, Naito Y, Colson S, Ichikawa A, Kudo T, Hayakawa A, et al. Experimental and numerical study of the laminar burning velocity of CH4-NH3-air premixed flames. Combust Flame 2018;187:185–98. https://doi.org/10.1016/j.combustflame.2017.09.002.
[48] Xiao H, Valera-Medina A, Bowen PJ. Study on premixed combustion characteristics of co-firing ammonia/methane fuels. Energy 2017;140:125–35. https://doi.org/10.1016/j.energy.2017.08.077.
[49] Klippenstein SJ, Mulvihill CR, Glarborg P. Theoretical Kinetics Predictions for Reactions on the NH2O Potential Energy Surface. Chem A Eur J 2023;127:8650–62. https://doi.org/10.1021/acs.jpca.3c05181.
[50] Klippenstein SJ, Harding LB, Ruscic B, Sivaramakrishnan R, Srinivasan NK, Su MC, et al. Thermal Decomposition of NH2OH and Subsequent Reactions: Ab Initio Transition State Theory and Reflected Shock Tube Experiments. Chem A Eur J 2009;113:10241–59. https://doi.org/10.1021/jp905454k.
[51] Dai LM, Gersen S, Glarborg P, Mokhov A, Levinsky H. Autoignition studies of NH3/CH4 mixtures at high pressure. Combust Flame 2020;218:19–26. https://doi.org/10.1016/j.combustflame.2020.04.020.
[52] Lubrano Lavadera M, Han XL, Konnov AA. Comparative Effect of Ammonia Addition on the Laminar Burning Velocities of Methane, n-Heptane, and Iso-octane. Energy Fuel 2021;35:7156–68. https://doi.org/10.1021/acs.energyfuels.0c03424.
[53] Zhu S, Xu Q, Tang R, Gao J, Wang Z, Pan J, et al. A comparative study of oxidation of pure ammonia and ammonia/dimethyl ether mixtures in a jet-stirred reactor using SVUV-PIMS. Combust Flame 2023;250:112643. https://doi.org/10.1016/j.combustflame.2023.112643.
[54] Li QS, Lü RH. Direction Dynamics Study of the Hydrogen Abstraction Reaction CH2O + NH2 → CHO + NH3. Chem A Eur J 2002;106:9446–50. https://doi.org/10.1021/jp026560x.